Research Article

iPSC-Derived Vascular Cell Spheroids as Building Blocks

for Scaffold-Free Biofabrication†

Leni Moldovan[1]

April Barnard[2]

Chang-Hyun Gil[3]

Y. Lin[3,4]

Maria B. Grant[5]

Mervin C. Yoder[3]

Nutan Prasain[3]

Nicanor I. Moldovan[6]

[1]Department of Surgery, Indiana University School of Medicine, Indianapolis, USA

[2]Department of Integrative Physiology, Indiana University School of Medicine, Indianapolis, USA

[3]Department of Pediatric Medicine, Indiana University School of Medicine, Indianapolis, USA

[4]Department of Biochemistry and Molecular Biology, Indiana University School of Medicine, Indianapolis, USA

[5]Department of Ophthalmology, Indiana University School of Medicine, Indianapolis, USA

[6]Department of Biomedical Engineering, IUPUI School of Engineering and Technology, Indianapolis, USA

Correspondence: Dr. Nicanor I. Moldovan, 3D Bioprinting Core Facility, IU School of Medicine, 980 Walnut St., 46202, Indianapolis, IN, USA

E-mail: nimoldov@iupui.edu

Abstract

Recently a protocol was established to obtain large quantities of human induced pluripotent stem cells (iPSC)-derived endothelial progenitors, called endothelial colony forming cells (ECFC), and of candidate smooth-muscle forming cells (SMFC). Here, we tested their suitability for assembling in spheroids, and in larger 3D cell constructs. iPSC-derived ECFC and SMFC were labeled with tdTomato and eGFP, respectively. Spheroids were formed in ultra-low adhesive wells, and their dynamic proprieties were studied by time-lapse microscopy, or by confocal microscopy. Spheroids were also tested for fusion ability either in the wells, or assembled on the Regenova 3D bioprinter by lacing them in stainless steel micro-needles (the 'Kenzan' method). We found that both ECFC and SMFC formed spheroids in about 24 hr. Fluorescence monitoring indicated a continuous compaction of ECFC spheroids, but which stabilized in those prepared from SMFC. In mixed spheroids, the cell distribution changed continuously, with ECFC relocating to the core, and showing pre-vascular organization. All spheroids had ability of in-well fusion, but only those containing SMFC were robust enough to sustain assembling in tubular structures. In these constructs we found a layered distribution of alpha smooth muscle actin-positive cells and extracellular matrix deposition. In conclusion, iPSC-derived vascular cell spheroids represent a promising new cellular material for scaffold-free biofabrication.

Abbreviations: ECFC, endothelial colony forming cells; **eGFP**, enhanced green fluorescent protein ;**EGM2**, endothelial growth medium 2; **HUVEC**, human umbilical cord endothelial cells; **iPSC**, induced pluripotent stem cells; **NRP1**, neuropilin 1; **PECAM-1**, platelet-endothelial cell adhesion molecule 1; **SMFC**, smooth-muscle forming cells; **VEGF**, vascular endothelial growth factor.

2

1 Introduction

Pre-assembled cell clusters, called 'spheroids' due to their spherical shape, are increasingly used for a variety of applications, from 3D normal or pathological tissue models [1] to biofabrication [2]. In particular, injection of pre-formed cell spheroids has been shown to increase cell survival and efficiency of pro-angiogenic cell therapy with both primitive [3] and adult [4] cells, as compared to single-cell suspensions. This holds true for cord-blood mesenchymal cells [5], as well as for a sub-class of circulating endothelial progenitor cells that are capable of forming colonies *in vitro*, which for this reason are named 'endothelial colony forming cells' (ECFC) [6].

Recently, Prasain et al. [7] established the protocol for large amplification (more than five orders of magnitude) of an endothelial progenitor cell lineage with cord blood ECFC properties, derived from human induced pluripotent stem cells (iPSC). ECFC of both cord and adult blood [8] or of iPSC [7] origin, are a very promising cell population for cardiovascular medicine [9]. Because their *in vivo* applications for cell therapy face the same biological constrains as other single-cell suspensions [5], it has been proposed to lead cells into alginate/fibrin microspheres [10]. However, this procedure requires complex preparations, followed by specialized bioreactor cultivation.

Alternatively, 'scaffold-free' (i.e., without embedding biomaterials) biofabrication uses only cells and their own extracellular matrix for creating bio-similar constructs [11]. Because the individual cells are very small, and also to give them the conditions to engage in phenotype-appropriate interactions and to secrete their own matrix, one approach is to directly pre-assemble cells into cell spheroids for biofabrication applications [2].

A key step in our iPSC-derivation protocol for ECFC is the selection by fluorescence-activated cell sorting of double-positive cells, based on the expression of CD31 (the platelet-endothelium cell adhesion molecule-1, PECAM-1), a cell surface molecule involved in homotypic interaction between the vascular endothelium and the

3

circulating leukocytes [12], and neuropilin-1 (NRP1), a co-receptor with vascular

endothelial growth factor (VEGF) receptor type 2, involved in endothelial signaling [7].

During this selection process, it was also discovered a population of iPSC-derived cells that

present CD31 on the surface, but not NRP1. Unlike the double positive cells, these

eventually express the alpha isoform of smooth-muscle-type actin, suggesting the

possibility that these cells are progenitors of vascular smooth muscle cells, or of myo-

fibroblasts. Although a more complete characterization of these cells is still in progress, by

taking into consideration their endothelial-supportive activity within the spheroids and

their integration in the tubular structures, as reported here, we suggest to similarly call

them 'smooth-muscle forming cells' (SMFC).

Given their possible complementary role in vascular biology and tissue repair, we

analyzed the preparation of spheroids from iPSC-derived ECFC and SMFC, labeled with the

fluorescent protein markers tdTomato and eGFP, respectively. We tested the ability of the

iPSC-derived ECFC and of their NPR1-negative SMFC counterparts to directly organize into

spheroids. An additional opportunity to assess their 3D assembling capacity in

meaningfully biofabricated constructs, was to use the Regenova bioprinting robot [13].

This instrument performs scaffold-free 3D assembling by replacing the biomaterial

scaffolding with a mechanical support, namely a Cartesian array of microneedles (the

'Kenzan' method) [14, 15]. Here we report on the properties and biofabrication potential

of these iPSC-derived cell spheroids, as well as their suitability for Kenzan bioprinting.

2 Materials and methods

2. 1 Cells isolation and labeling. Human iPSC and ECFC were obtained and

expanded by a published method [7]. NRP1$^-$CD31$^+$ cells were obtained in the same

selection as the NRP1$^+$CD31$^+$ cells. These cells were transduced with a lentiviral vector to

4

express eGFP (green) and tdTomato (red), respectively. Both cell types were routinely maintained in complete EGM-2 medium (Lonza).

2.2 Spheroids formation. Labeled cells were seeded in EGM-2 in ultra-low adhesive U-bottomed 96 well plates (Sumitomo Bakelite, Tokyo, Japan). In preliminary experiments we determined that 2.5×10^4 cells/well produce within 24 h spheroids of about 0.5 mm diameter, as required for Regenova bioprinting. This initial cell number was maintained for preparation of spheroids throughout the experiments. To test their propensity for fusion, after separate formation the spheroids were placed in the same wells for up to 72 h.

2.3 Spheroids imaging and analysis. After seeding, the plates were monitored every 4 h for 72 h in the automated microscope IncuCyte Zoom® (Essen Bioscience). At the end of the incubation the spheroids were imaged in combined transmission/fluorescence microscopy (Leica DMIL), or in a confocal Olympus FV1000 MPE microscope.

2.4. Kenzan bioprinting. For bioprinting, we used spheroids compacted for 24 h. In brief, the Kenzan method performed by the Regenova bioprinting consists of gentle aspiration of individual spheroids from their formation wells, and placing them in contact by implantation in stainless steel micro-needles ('kenzans'), of 170 µm in diameter (**Fig. S1**, and [14]). These microneedles are arranged in a Cartesian pattern with a hollow central space, which allowed the perfusion of fresh EGM2 medium. The construct was maintained for seven days in the needle array to enable spheroids to fuse and produce extracellular matrix, in a perfusion bioreactor operated at a flux of 4 mL/min [13].

2.5. Immunostaining. At the end of this incubation, the construct was removed and either directly imaged in fluorescence microscopy, or fixed in 4% paraformaldehyde, embedded in OCT, and then sectioned on a Leica microtome. Sections were stained with antibodies to alpha smooth muscle actin (from eBioscience) or collagen type IV (from Abcam), and counter-stained with DAPI for nuclei localization.

5

3 Results

3.1 Formation of compact vascular cell-containing cell spheroids. Seeding of NRP+CD31+ ECFC in ultralow-adhesive, U-shaped well culture plates [16, 13] produced 'cell lawns' with a scattered yet slightly clumped pattern (**Fig. 1A** top). These colonies eventually led to formation of spheroids, but they were not uniformly compacted and were imperfectly round (**Fig. 1A**, bottom and **Fig. S2**).

At the same time, eGFP+/NRP1-CD31+ (SMFC) cells formed rounder discs (**Fig, 1B**, top), which eventually condensed in almost spherical cell clusters (**Fig. 1B**, bottom). For this reason, we then combined the two cell populations, to determine whether SMFC could provide the ECFC with the needed support for generation of better spheroids. Indeed, the mixed tdTomato+-ECFC/eGFP+-SMFC colonies (**Fig. 1C** top) eventually formed spheroids with the same compact shape (**Fig. 1C**, bottom) as the eGFP/NRP1-CD31+ only cells. Moreover, when we compared the frequency of imperfectly formed spheroids, we found that this was higher in ECFC-only spheroids than in SMFC-only spheroids, while the mixed colonies generated the highest number of well-rounded, compact spheroids (**Fig. S2**).

Time-lapse microscopy of mixed spheroids indicated that the spheroids assembling was complete at 24 h (**Fig. 1D**; result corroborated with data in **Fig. 2**). However, their composition continued to change, with an increase in the proportion of eGFP+/NRP1-CD31+ cells (**Fig. 1D**, compare the early and late frames), suggestive of ECFC translocation from the surface toward spheroid's core and/or reduction of their proportion.

3.2 Quantifying spheroid size and composition. Taking the spheroids in use prematurely, i.e., insufficiently compacted, may lead to failed assembling or to biofabricated constructs with suboptimal properties. Therefore, it is important to know when their size and cellular composition stabilizes, considering the possible cell turnover by proliferation and death. To this end, we measured the area of fluorescent images in all

6

three conditions (**Fig. 2A**). This analysis confirmed that, although all spheroids were made from the same initial number of cells, ECFC spheroids were not only more irregular, but also smaller (compare with **Figs. 1A** and **S2**). In addition, we found that after a rapid shrinkage, the size of SMFC-containing spheroids stabilized after about 18 h, while that of ECFC-only continued to decrease (**Fig. 2A**). Considering the starting cross-sectional area, there were small differences in the magnitude of the effect; however, while ECFC alone (red line) kept decreasing for the duration of the experiment, the SMFC (green line) alone and mixed (purple) lines plateaued. In addition, when we compared the rates of the size changes in ECFC, we observed clear differences between these in the initial hours (**Fig. S3**). Remarkably, the size of mixed spheroids remained always larger than that of ECFC only, and also stabilized, while showing an even slight upward trend (**Fig. 2A**).

We also quantified the intensity of spheroids fluorescence on the two channels. This is proportional to the number of respective emitting cells, and was found to be dependent on the time in culture. This quantification enabled us to compare the behavior of each cell type, as well as with the superficial (**Fig. 1D**) vs. overall (**Fig. 3**, *vide infra*) cell proportions within spheroids. We found that the fluorescence intensity produced by the spheroids composed of ECFC alone decreased more rapidly (**Fig. 2B**, red line). On the other hand, the red fluorescence produced by the tdTomato positive ECFC was more stable in mixed spheroids (**Fig. 2B**, purple line). This difference in the rate of fluorescence change was better documented by the two curves' derivatives, which showed the 'speed of change' (**Fig. S3**). The fluorescence produced by the eGFP+ SMFC either alone (**Fig. 2C**, green line) or in combination (**Fig. 2C**, purple line) slightly increased and stabilized in the first two days, after which it started to decline. This data suggested that ECFC-only clusters are structurally more unstable than those prepared from SMFC alone, but the latter can provide them some form of protection when in mixed spheroids.

7

3.3 Cellular relocation within spheroids. One of the conspicuous properties of cell-heterogeneous spheroids is 'cell sorting', namely separation of cell layers based on their affinity, those with increased adhesiveness tending to compact together at the spheroid core [17]. Since (i) adult endothelial cells remain at the surface of mixed spheroids [18, 19], and (ii) ECFC manifest a reduced intercellular adhesiveness in the early stages of aggregation (**Fig. 1A** vs. **1B**), we anticipated that ECFC would also prefer a *superficial* distribution. Instead, after initially displaying the expected surface localization, the proportion of superficial ECFC surprisingly decreased, and consequently the majority of the cells eventually visible at the exterior were those eGFP-positive (**Fig. 1D**). This process was confirmed by imaging the spheroids at higher magnification (**Fig 3A**).

Notably, **Fig. 3B** suggests superficial ECFC accumulations and also incipient formation of cell 'cords', as part of the cellular dynamics in these structures at early time points (1 day), unlike the corresponding SMFC (**Fig. 3C**). Optical sectioning by confocal microscopy of two weeks-old spheroids revealed an almost complete 'cell sorting', with cortical distribution of SMFC, and ECFC concentrated at the core (**Fig. 3D-F**). The structured organization of ECFC at the core of these spheroids suggested generation of cell cords (**Fig. 3B**), and also possible a sprouting-like activity (**Fig. 3D-F**).

3.4 SMFC-containing spheroids can be assembled in larger structures by scaffold-free biofabrication. Next, we assessed whether the iPSC-derived spheroids can undergo fusion either independently, or after being laced together in larger structures. To this end, we first placed together separately-formed spheroids in one well. We found that indeed their fusion took place and progressed at a pace dependent on the cluster size. Namely, the fusion process was faster and more complete when the number of spheroids brought together was smaller (**Fig. 4A-B** vs. **4C-D**).

To keep the spheroids in stronger contact, for longer intervals and in larger assemblies, we employed the Regenova Bio 3D-Printing robot [15]. This instrument

8

'impales' pre-formed half-millimeter spheroids one-by-one in stainless steel microneedles ('kenzans'[14]) (**Fig. S1**). Consequently, the spheroids are skewered in contact to each other, an interaction that would promote their eventual fusion in a tissue-like structure by cell translocation and further matrix secretion. In accordance with the observations in individual spheroids, the ECFC retained the ability to fuse and form cell cords after their assembling in the kenzans (**Fig. 4E**), unlike the co-embedded SMFC (**Fig. 4F**).

      3.5 Mixed bio-assembled spheroids show signs of vascular differentiation. Our attempts to permanently lace cell spheroids made only from the ECFC by this method have failed, consistent with their poor aggregation capacity (**Fig. 1**). Instead, those made from NRP1-CD31+ cells were more Kenzan-printable. Their consistency was strong enough to resist the gentle aspiration by the nozzle connected to the robotic arm of the bioprinter, as well as the piercing by the sharp microneedles (**Fig. S1B** and **Fig. 4E-F**). The constructs were maintained in micro-needle arrays with a hollow space, which allowed continuous perfusion of the tubular construct with fresh medium [13]. After 7 days, the tubes thus formed were removed, fixed, and either imaged as such by transmission (**Fig. 4G**) or fluorescence microscopy (**Fig. 4H**). Alternatively, the tubes were maintained another 7 days in culture, after which they aey were fixed, paraffin-embedded and immuno-stained (**Fig. 5**). Based on the distribution of DAPI-positive nuclei, this construct proves to be a densely-populated cellular structure, many of the cells still expressing the eGFP marker in various degrees (**Fig. 4F, 5A**). However, their distribution was rather sparse, with spaces likely occupied by other cells, or by an extracellular matrix rich in collagen type IV (**Fig. 5B**). Remarkably, this construct also presented a layered distribution of smooth-muscle actin-expressing cells (**Fig. 5C, D**). These were distributed either closer to the interior, or to the exterior of the tube, but were largely missing in the middle section (**Fig. 5D**).

4 Discussion

Cell clusters are ubiquitous in nature and in various biotechnological applications, because the cells perform their functions in interaction with each other. Many of the basic mechanisms of spheroid generation and layered organization are present in developmental biology [20] and tumor formation [21]. Although normal-cell spheroids do not seem to spontaneously occur or fuse in the adult body, this primitive self-assembling mechanism, present in embryos [22] has been proposed [2] and largely exploited for tissue engineering [1], including for vascular constructs [23, 24, 25], as we are doing in this study. The 'organoids' are also basically cell spheroids that recapitulate tissue development, thus opening new opportunities for regenerative medicine [26], while spheroids prepared from adult cells are increasingly used in biofabrication applications, from augmented cell therapy [5, 3], to vascular grafts [11, 27, 28] and to 3D bioprinting [2, 29, 2, 30, 31].

One of the most advanced biofabrication methods is bioprinting. Traditionally, bioprinters required a cell-embedding 'scaffold' biomaterial, called for this reason bioink [32]. In this form of bioprinting, one must take into consideration first the biomaterial's suitability for dispersion by the bioprinter and second its role as biological support. Depending on the type of bioprinting (ink-jet, extrusion or laser-assisted), there are different reasons for which the efficiency of scaffold-dependent bioprinting remains low, and its anticipated translation to clinic still uncertain [14, 33].

For this reason, much effort is being currently put into scaffold-free bioprinting methods. One is the 'Kenzan' method which laces and temporarily keeps cell spheroids in microneedle arrays until they fuse in larger constructs [15, 13]. However, finding the cells capable to produce spheroids with suitable properties for scaffold-free biofabrication, and for the Kenzan method, remains an empirical undertaking [14].

10

Recently Prasain *et al.* established a method to produce large quantities of ECFC from iPSC [7]. This progress opens the way towards personalized biofabrication, combined with other cell types, of autologous tissue-engineered constructs. It also creates the opportunity for efficient clinical treatments by cell therapy, beyond the cardiovascular realm, of a variety of circulation-dependent diseases. Essentially, this method consists of isolation, after appropriate priming, of a subpopulation of NRP1$^+$CD31$^+$ cells by fluorescence activated cell sorting [7]. A class of NRP1$^-$CD31$^+$ cells, of less defined phenotype is produced during this operation. Unlike ECFC, these cells express smooth muscle-type actin [7]. This suggests their potential to differentiate into a vascular smooth muscle cell/fibroblast lineage.

4.1 Formation of cell spheroids. Vascularization of engineered tissues is essential for their survival, but it has remained a stumbling block in this field [34]. The investigation of endothelial cells as spheroid components is therefore a necessary step. Human umbilical endothelial cells (HUVEC)-only spheroids were previously reported, despite the epithelial nature of these cells [4], but at the spheroid's core they eventually died by 'anoikis' (a form of apoptosis triggered by the lack of attachment to a solid substrate), while those on the surface survived [18].

In contrast, mixed spheroids made of human dermal microvascular endothelial cells and osteoblasts formed vessel-like networks within 72 h, and showed a decrease in apoptosis as compared to endothelial-only spheroids [35]. These mixed spheroids were also larger in size when compared to single cell-type spheroids, even after transplantation, when microvascular primordia emerged from the spheroids and connected to the host microcirculation [35]. Similarly, the spheroids prepared from HUVEC and smooth muscle cells [36] had less apoptosis than those made from HUVEC alone [18]. Again, at their cores endothelial cell cords could be readily detected. Altogether, these findings indicate that mixed cell spheroids containing endothelial cells (i) preserve their viability, (ii) promote

11

3D organization and proliferation, and (iii) sustain neovascularization *in vivo*. Therefore, they may be used as functional vascularization units for cell therapy and tissue engineering.

Here we used ECFC as a more primitive cell type, with a higher propensity to proliferation and differentiation than the HUVEC (which as fetal tissue, are by necessity closer to the termination of their biological role). We report that ECFC have the ability to quickly aggregate in relatively round clusters in non-adhesive culture wells. However, when prepared from ECFC alone, these cell clusters were loose and their size constantly decreased. In addition, they had poor biomechanical consistency, as shown by the inability to be sustain integrity when gently aspirated with the low depression routinely used by the Regenova's robotic arm, and to sustain the implantation in the instrument's microneedles. To prepare more robust spheroids from ECFC only, we could have considered other methods to strengthen their intercellular interactions (such as using magnetic beads [37]), or to incorporate them in biomaterials as additional extracellular matrices [10]. However, we considered that a compact mass of cells, even at the progenitor stage, is an unusual situation for the normal epithelial physiology. Instead, we were more interested in assessing the properties in this respect of the also available NRP1$^-$CD31$^+$ cell population either in making spheroids by themselves, or as potential 'carriers' of the ECFC. Indeed, we found that SMFC formed more robust spheroids, which maintained their sturdiness even when replaced by up to 20% ECFC. Moreover, SMFC appeared to provide protection to ECFC, even after these relocated to the core of spheroids, where they seemed to further differentiate into pre-vascular cords.

4.2 Spheroids geometry. Spheroid shape and size are defining, and often critical, properties for many tissue engineering applications. For example, diffusion of oxygen and nutrients depend on spheroid size, thus impacting on cell survival and differentiation. In Kenzan bioprinting, the spheroids must be spherical in order to precisely fit the mouth of

12

the nozzle which takes them from the formatting wells. Also, to come in contact with each other for subsequent fusion, these spheroids need to be uniform in size and with a diameter comparable with the distance between micro-needles [14]. For these reasons, spheroid shape and size are the first 'quality check' on the Regenova bioprinter, wherein those non-conform to these standards are rejected out of the actual printing.

Due to the very processes leading to their formation, mainly the system's energy decrease via maximal attraction and optimal cell redistribution [38], the spheroids continuously shrink. However, the pace of size reduction slows down or even ceases, due to the concurring forces derived from compaction (given the constant cell volume), combined with the resultant of cell turnover (i.e., cell proliferation and cell death). Therefore, finding the correct timing to attain a reasonably stable spheroid diameter is an important consideration for their optimal use in biofabrication. If the spheroids are used too early, they might not be fully formed in terms of intracellular interactions and extracellular matrix composition, and thus not enough robust during subsequent manipulation. Conversely, keeping them too long in culture could make them vulnerable to hypoxia and nutrient depletion at the core [39]. In our hands, all three spheroid types attained their relatively stable size within 18-24 h, with much of their compaction occurring during the first 3 h. This seems to be comparable, or faster than for other cells types, which for the same purpose might take several days [40].

4.3 Cell turnover in spheroids. We also found that even in this short interval, the cell ratio within spheroids significantly changed. Surprising and still not fully explained, was the apparent cell loss in spheroids made of ECFC only. The growth medium is unlikely to account for this effect, given that it was optimized for their cultivation, and that NRP1$^-$CD31$^+$ cell spheroids paradoxically thrived in this medium. A more likely explanation is that 3D compaction is an un-physiological situation for the endothelial phenotype, as previously shown for HUVEC [18]. In addition, through the combination of poor

13

oxygenation and nutrient depletion, the compaction collectively produced an ischemic condition, routinely found at the core of spheroids larger than 400 μm. The limit of oxygenation diffusion *in vivo* is 200 μm [41]. This finding is not unexpected, also given the known benefit of a stirred bioreactor to keep ECFC alive, when packed within fibrin microspheres [10].

We also found that NRP1⁻CD31⁺ cells protected the ECFC against their apparent decay within spheroids. These SMFC may either (i) provide an environment rich in supporting paracrine growth factors or (ii) secrete an extracellular matrix that allows the ECFC to penetrate and/or organize in pre-vascular cords, thus promoting their maturation. At the same time, we noticed that adding ECFC up to 20% among SMFC did not change much the dynamics of the 'host' cells in these mixed spheroids, supporting the structural and biological robustness of NRP1⁻CD31⁺ cells.

In mixed spheroids, the final cell positioning, called 'cell sorting' due to their layered distribution, depends on biophysical parameters such as the strength of inter-cellular interactions [42]. During embryogenesis cell sorting explains the formation of primitive germ layers within the embryo [43]. Cell migration following chemotactic gradients is also likely to occur in ECFC spheroids. Based on their more disperse, unstructured initial colonies and looser spheroids, they would have been expected to have a reduced intercellular attachment, which in turn predicted their localization at the periphery. Instead, we observed a paradoxical accumulation of ECFC at the spheroid core. This could be the result of ECFC chemo-tropism towards the hypoxic core, likely mediated by a VEGF concentration gradient [44]. Arriving there, ECFC may undergo further maturation under the influence of VEGF [7]. That would also explain the apparent sprouting from the ECFC cords, characteristic to an actively proliferating endothelium. We did not directly explore this mechanisms, however we speculate that the more primitive

14

nature of ECFC as compared to EC makes them more chemotactically sensitive to the VEGF possibly generated at the hypoxic spheroid core [44].

4.4 Biofabrication with spheroids. EC/SMC spheroids have been previously used for assembling by 'scaffold-free biofabrication' of vascular grafts [13], but not when derived from iPSC. This method enables the acquiring of high quantities of cells in a relatively short time, which represents a clear advantage. Therefore we verified the ability of our spheroids to fuse in the culture wells, and we also tested their 'printability' on the Regenova robot. Besides appropriate size and shape, the spheroids needed to be sturdy enough for handling for this method, both during uptake and their piercing by the micro-needles. While the ECFC alone did not pass this test, SMFC either alone or in combination with ECFC were capable to sustain this form of biofabrication. Large vessels are essentially composed of a thick layer of smooth muscle cells. This implies that, with further improvements, these spheroids could be eventually used as building blocks of scaffold-free biofabrication of vascular grafts. Moreover, SMFC-only spheroids could represent an interesting cellular system for cell therapy, through their ability to stimulate and/or support the micro-vascular development *in vivo* via paracrine factors.

4.5 Towards vascular differentiation of constructs. The robust expression of alpha smooth muscle actin and collagen IV (a major component of vascular basement membrane [45]) in our tubular constructs maintained post-printing in a perfusion chamber, sustains their anticipated use as vascular grafts. In this regard, an unexpected finding was the layered distribution of smooth muscle actin towards both inner and outer surfaces. This could be the result of the construct's exposure to fluid shear stress in the bioreactor, since it is well established that the expression of this marker in vascular cells is inducible by biomechanical cues [46].

Admittedly, more markers are needed to be assessed, as well as more biomechanical testing of the spheroids and the ensuing constructs. Thus, our tubular

15

constructs were not yet ready for biomechanical testing *in vitro*, or in an *in vivo* setting. One reason is the insufficient structural cohesion, due at least in part to the lack of elastic elements (elastin sheets and/or collagen I production), to provide them with the required resistance and compliance. In fact, these properties were insufficient even when adult smooth muscle cells and fibroblasts were used for spheroids preparation [13]. This limitation could be addressed by, e.g., (i) more specifically drive the differentiation of our cells towards a medial phenotype, or (ii) the use of 'hybrid' bioprinting, which would allow incorporation in the construct of stronger biomaterials, such as polymeric fibrillar scaffolds [47].

In conclusion, here we show that cell spheroids with promising properties for scaffold-free biofabrication can be prepared from iPSC-derived vascular progenitors. We found the optimal maturation time for spheroids collection, and investigated relevant cellular dynamic properties. Remarkably, the mixed spheroids demonstrated improved properties and long-term vitality at the core, and seemed to encapsulate microvascular fragments ready for larger-scale bio-assembling. In addition, we preliminarily found these spheroids' suitability for 'scaffold-free' bioprinting, using the Kenzan method on the Regenova instrument.

Conflict of interest

The authors declare no financial or commercial conflict of interest.
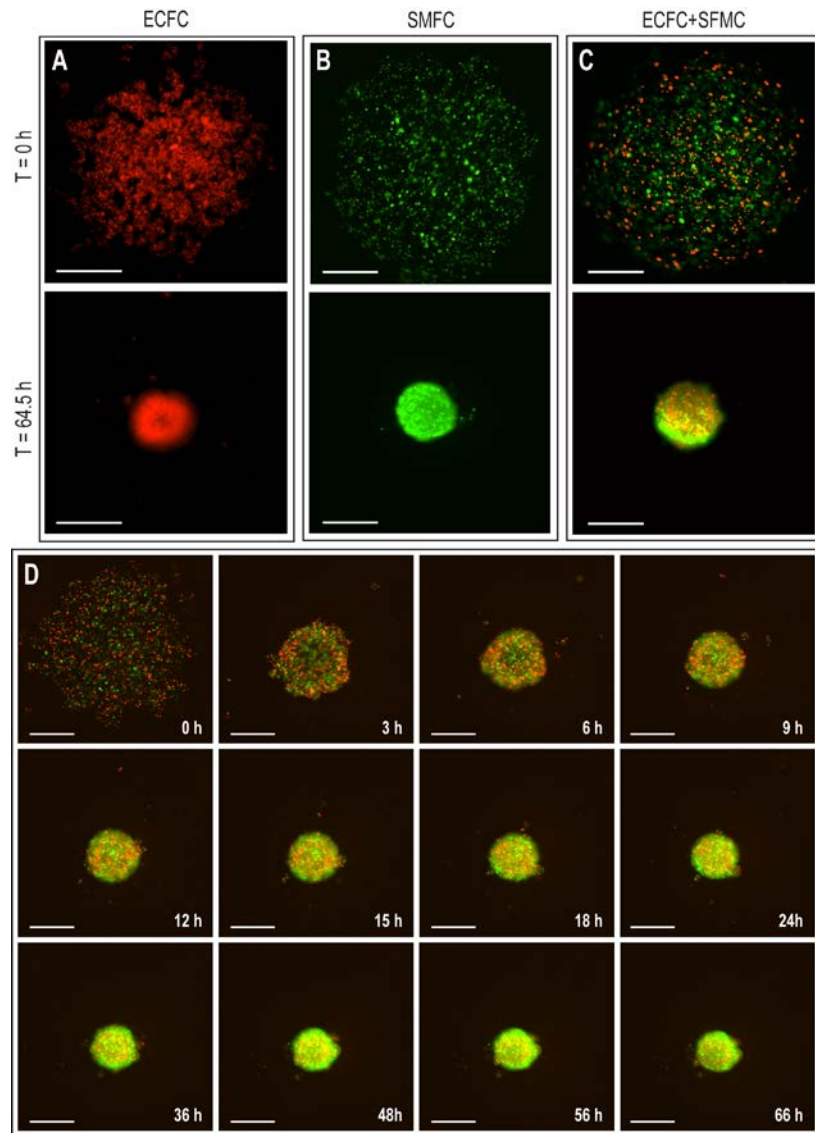
Figure legends

Figure 1. Assembling of iPSC-derived vascular cells into spheroids. A. tdTomato labeled iPSC-derived ECFC settle as diffuse colonies (top), and form irregular spheroids (bottom) in U-shaped low-adhesive plates. **B**. eGFP-expressing $NRP1^+CD31^+$ make rounder colonies (top), then aggregate in well-defined spheroids (bottom). **C**. Mixed 1:5 populations of iPSC-derived ECFC and SMFC behave more similarly to their SMFC-only counterparts. **A-D**, representative images, selected from 80-90 spheroids/condition. **D.** Time-lapse snapshots of formation of a mixed spheroid composed of iPSC-derived ECFC-tdTomato and eGFP-SMFC. A relatively stable spheroid size was attained in ~18 h, but the cell proportions on the surface changed from predominantly ECFC (red) at 9 h, to mostly SMFC (green) at 48 h. Magnification bars: 500 μm.
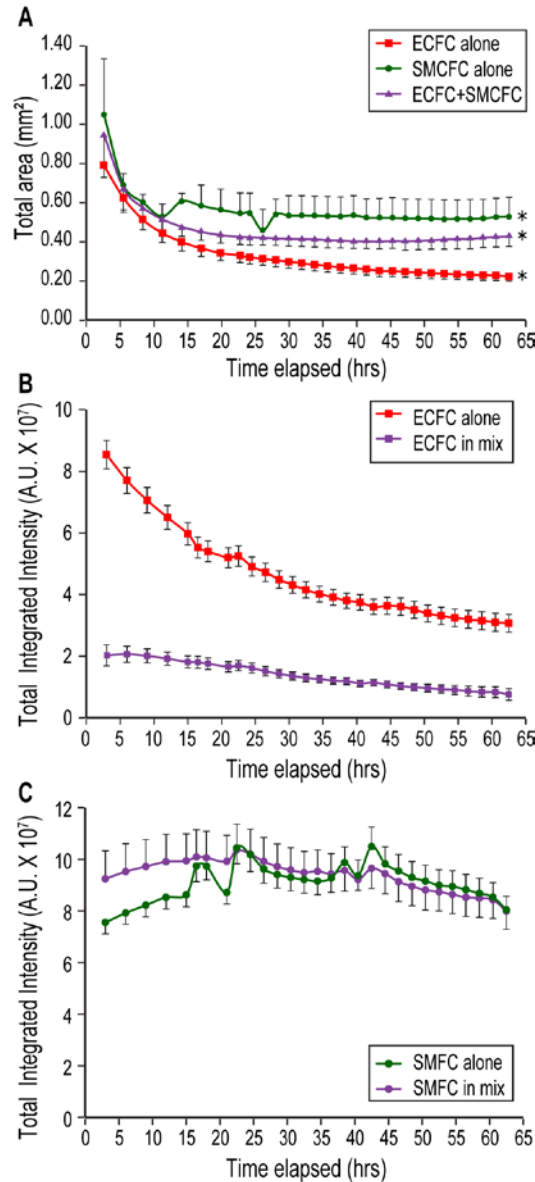
18

Figure 2. Tracking the changes in spheroids cellular composition. A. Time course of spheroids size as inferred from their fluorescence images. Red line, ECFC (n = 57); green line, SMCS (n = 87); purple line, mixed in the proportion 1:5 (red/green) (n = 93). Data are means ± SD. *****, p < 0.001 for all comparisons at the end of the incubation. **B**. Time course of integral fluorescence of spheroids made from ECFC only (red line, n=57), and of tdTomato fluorescence in mixed 1:5 ECFC/SMFC spheroids (purple line, n=93). **C.** Fluorescence of the spheroids prepared from eGFP^{+}/NRP1^{-}CD31^{+} cells (green line, n=87), and of the eGFP in mixed spheroids (purple line, n=93). The plates were seeded with cells from the same batch and processed and imaged in parallel. In **B** and **C**, data represent mean integrated intensity/image ±SD.
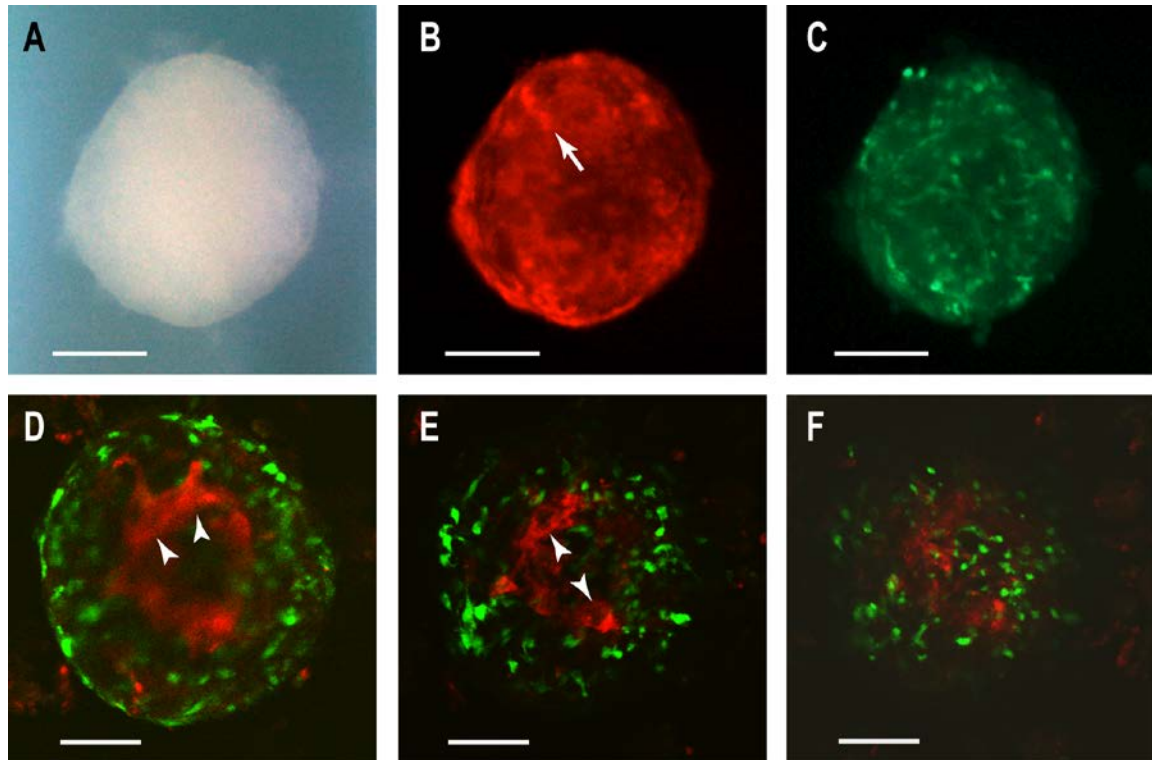
19

Figure 3. Cell distribution in early vs. late spheroids. A. Phase contrast imaging of a one-day old spheroid of mixed cell composition. **B.** Radial positioning of a tdTomato-positive iPSC-ECFC cell cord within this same spheroid (arrow). **C.** Corresponding eGFP-expressing SMFC in the same spheroid. **D-F.** Successive confocal sections through a one-week old spheroid: note the extensive 'cell sorting' (layered separation), and the organization of the ECFC in a fashion suggestive of cell cord formation, with possible sprouting viewed longitudinally (in **D**, arrowheads), or transversally (in **E**, arrowheads). Bars: **A-C**, 200 μm; **D-F**, 100 μm.
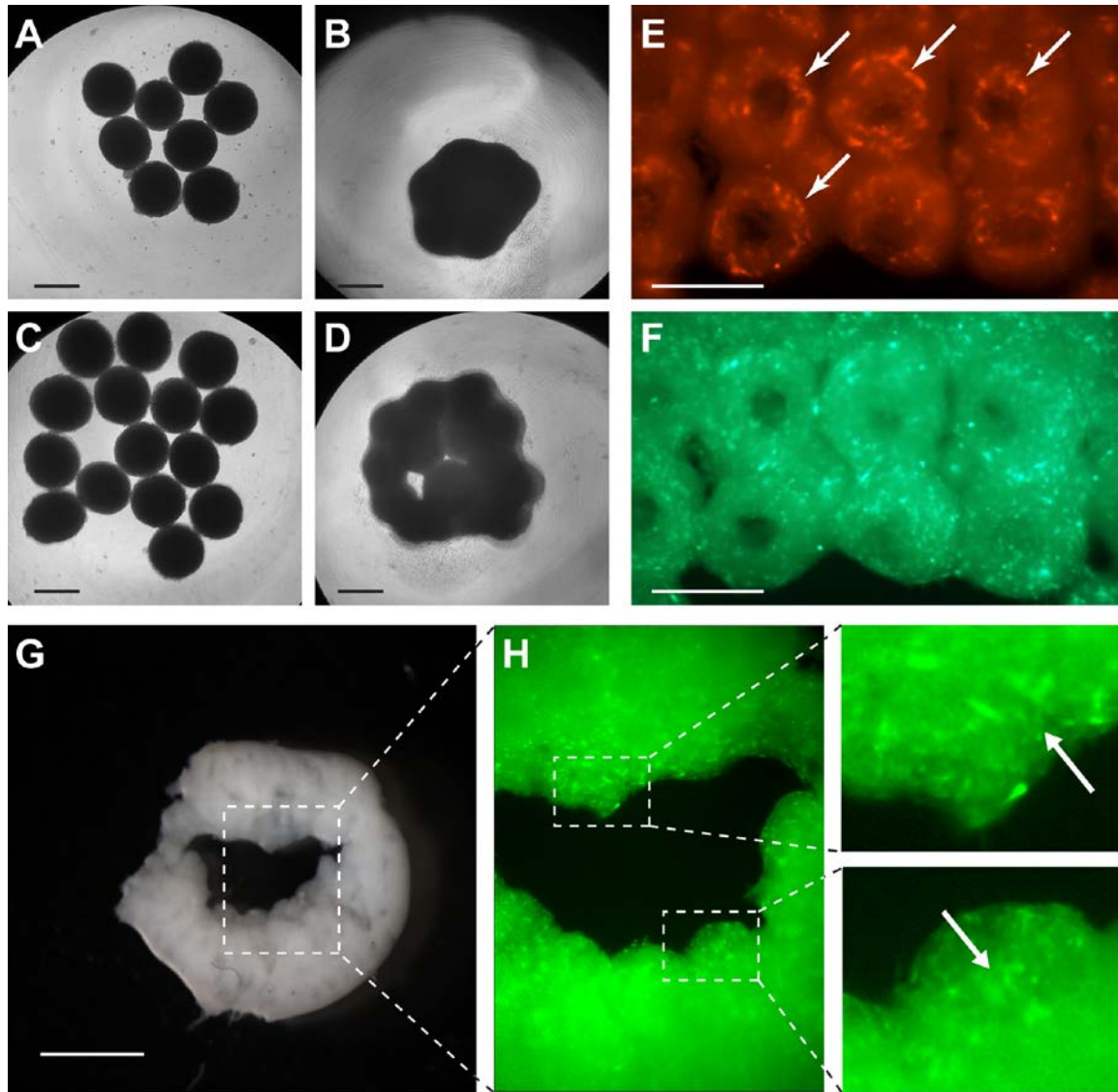
Figure 4. Fusion and internal organization of iPSC-derived spheroids in wells and upon printing. A. In-well fusion of eight (**A**, **B**) and 15 (**C**, **D**) 24 h-old spheroids, composed of 1:10 ECFC/SMFC. **A**, **C**: Time 0; **B, D**: 48 hrs. **E, F.** Assembled mixed cell spheroids at their removal from micro-needles**. E:** Cord-like circular organization of ECFC (red) in spheroids. **F**: Corresponding SMFC distribution (green). **G.** Micro-photograph of the construct at one week post-printing. **H.** Whole-mount fluorescence microscopy, showing the eGFP-expressing cells (arrows, in the inserts), embedded in abundant, newly-secreted ECM (pale-green, auto-fluorescence). Magnification bars, 500 μm.
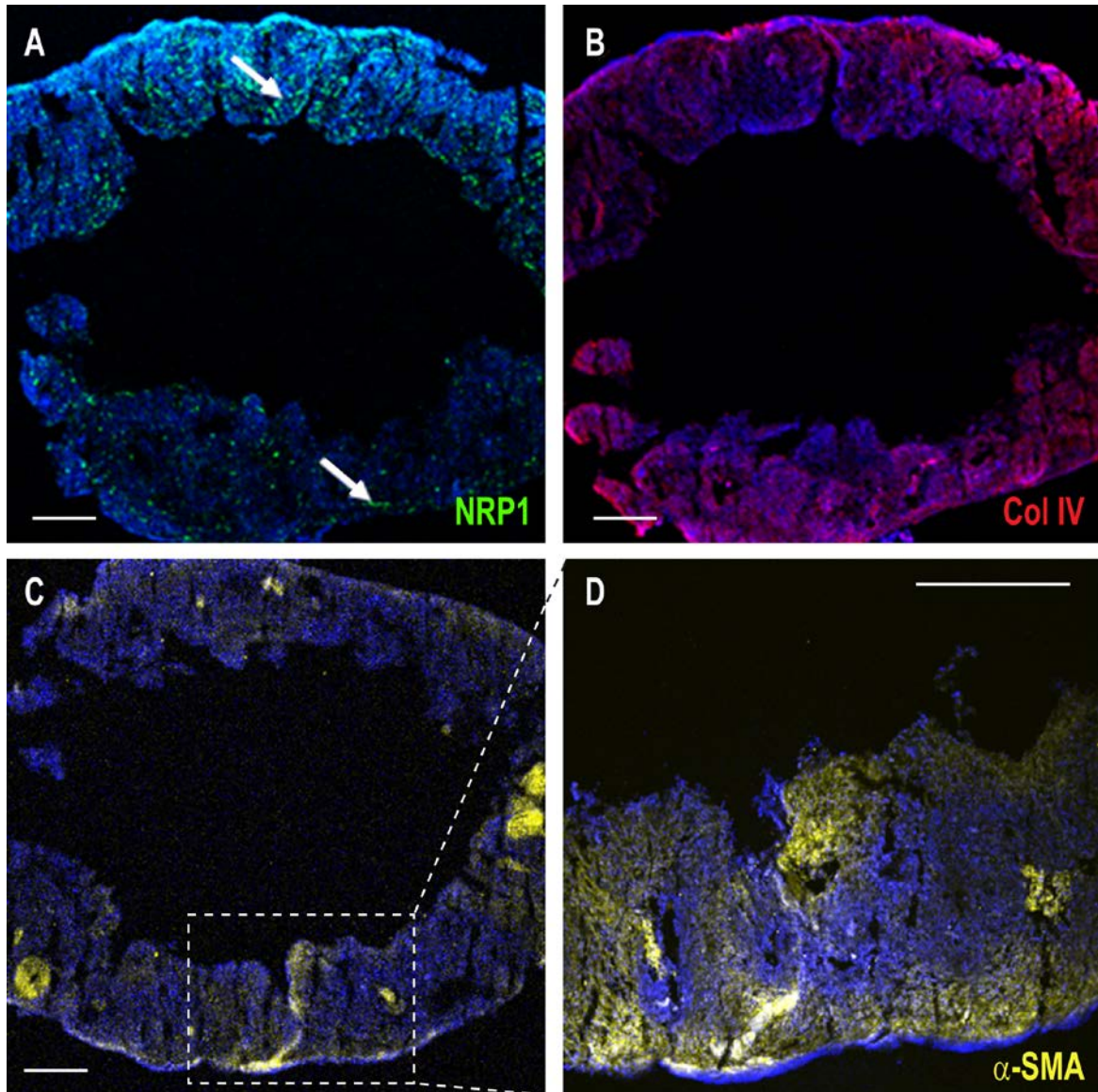
Figure 5: Characterization of a construct prepared from iPSC-derived SMFC at one week after removal from the kenzan needles. A. Confocal microscopy of the construct, identifying the eGFP-positive SMFC (arrows). **B.** Adjacent section with immunostaining for collagen type IV (red). **C.** Alpha-smooth muscle actin positive (yellow) and negative (fibroblastic) cells, the former being more concentrated on the surfaces of the construct. **D.** Higher magnification of **C**. In **A-D** blue, DAPI staining. Magnification bars, 1 mm.

References

1. M. W. Laschke, M. D. Menger, *Trends Biotechnol.* **2017**, *35*, 133.

2. V. Mironov, R. P. Visconti, V. Kasyanov, G. Forgacs, C. J. Drake, R. R. Markwald, *Biomaterials.* **2009**, *30*, 2164.

3. S. H. Bhang, S. W. Cho, W. G. La, T. J. Lee, H. S. Yang, A. Y. Sun, S. H. Baek, J. W. Rhie, B. S. Kim, *Biomaterials.* **2011**, *32*, 2734.

4. S. H. Bhang, S. Lee, T. J. Lee, W. G. La, H. S. Yang, S. W. Cho, B. S. Kim, *Tissue Eng Part A.* **2012**, *18*, 310.

5. S. H. Bhang, S. Lee, J. Y. Shin, T. J. Lee, B. S. Kim, *Tissue Eng Part A.* **2012**, *18*, 2138.

6. P. J. Critser, M. C. Yoder, *Curr. Opin. Organ Transplant.* **2010**, *15*, 68.

7. N. Prasain, M. R. Lee, S. Vemula, J. L. Meador, M. Yoshimoto, M. J. Ferkowicz, A. Fett, M. Gupta, B. M. Rapp, M. R. Saadatzadeh, M. Ginsberg, O. Elemento, Y. Lee, S. L. Voytik-Harbin, H. M. Chung, K. S. Hong, E. Reid, C. L. O'Neill, R. J. Medina, A. W. Stitt, M. P. Murphy, S. Rafii, H. E. Broxmeyer, M. C. Yoder, *Nat. Biotechnol.* **2014**, *32*, 1151.

8. N. Prasain, J. L. Meador, M. C. Yoder, *J. Vis. Exp.* **2012**, 62, 3872.

9. P. J. Critser, S. L. Voytik-Harbin, M. C. Yoder, *Cell Prolif.* **2011**, *44 Suppl 1*, 15.

10. J. K. Gandhi, L. Zivkovic, J. P. Fisher, M. C. Yoder, E. M. Brey, *Sensors. (Basel).* **2015**, *15*, 23886.

11. A. Shafiee, M. McCune, G. Forgacs, I. Kosztin, *Biofabrication.* **2015**, *7*, 045005.

12. W. A. Muller, S. A. Weigl, X. Deng, D. M. Phillips, *J. Exp. Med.* **1993**, *178*, 449.

13. M. Itoh, K. Nakayama, R. Noguchi, K. Kamohara, K. Furukawa, K. Uchihashi, S. Toda, J. Oyama, K. Node, S. Morita, *PLoS. One.* **2015**, *10*, e0136681.

14. N. I. Moldovan, N. Hibino, K. Nakayama, *Tissue Eng Part B Rev.* **2017** *23*, 237.

15. T. Shimoto, K. Nakayama, S. Matsuda, Y. Iwamoto, *Journal of Robotics and Mechatronics.* **2012**, *24*, 347.

16. R. Noguchi, K. Nakayama, M. Itoh, K. Kamohara, K. Furukawa, J. Oyama, K. Node, S. Morita, *J. Heart Lung Transplant.* **2016**, *35*, 137.

17. D. A. Beysens, G. Forgacs, J. A. Glazier, *Proc. Natl. Acad. Sci. U. S. A.* **2000**, *97*, 9467.

18. T. Korff, H. G. Augustin, *J. Cell Biol.* **1998**, *143*, 1341.

19. L. Pfisterer, T. Korff, *Methods Mol. Biol.* **2016**, *1430*, 167.

20. J. C. Mombach, J. A. Glazier, *Phys. Rev. Lett.* **1996**, *76*, 3032.

21. E. C. Costa, A. F. Moreira, D. de Melo-Diogo, V. M. Gaspar, M. P. Carvalho, I. J. Correia, *Biotechnol. Adv.* **2016**, *34*, 1427.

22. R. A. Foty, M. S. Steinberg, *Dev. Biol.* **2005**, *278*, 255.

23. T. R. Olsen, B. Mattix, M. Casco, A. Herbst, C. Williams, A. Tarasidis, D. Simionescu, R. P. Visconti, F. Alexis, *Acta Biomater.* **2015**, *13*, 188.

24. B. M. Mattix, T. R. Olsen, M. Casco, L. Reese, J. T. Poole, J. Zhang, R. P. Visconti, A. Simionescu, D. T. Simionescu, F. Alexis, *Biomaterials.* **2014**, *35*, 949.

25. B. Mattix, T. R. Olsen, Y. Gu, M. Casco, A. Herbst, D. T. Simionescu, R. P. Visconti, K. G. Kornev, F. Alexis, *Acta Biomater.* **2014**, *10*, 623.

26. K. R. Koehler, E. Hashino, *Nat. Protoc.* **2014**, *9*, 1229.

27. J. Groll, T. Boland, T. Blunk, J. A. Burdick, D. W. Cho, P. D. Dalton, B. Derby, G. Forgacs, Q. Li, V. A. Mironov, L. Moroni, M. Nakamura, W. Shu, S. Takeuchi, G. Vozzi, T. B. Woodfield, T. Xu, J. J. Yoo, J. Malda, *Biofabrication.* **2016**, *8*, 013001.

28. M. McCune, A. Shafiee, G. Forgacs, I. Kosztin, *Soft. Matter.* **2014**, *10*, 1790.

29. K. Jakab, C. Norotte, F. Marga, K. Murphy, G. Vunjak-Novakovic, G. Forgacs, *Biofabrication.* **2010**, *2*, 022001.

30. K. Jakab, A. Neagu, V. Mironov, R. R. Markwald, G. Forgacs, *Proc. Natl. Acad. Sci. U. S. A.* **2004**, *101*, 2864.

31. K. Jakab, A. Neagu, V. Mironov, G. Forgacs, *Biorheology.* **2004**, *41*, 371.

32. A. Skardal, A. Atala, *Ann. Biomed. Eng.* **2015**, *43*, 730.

33. S. V. Murphy, A. Atala, *Nat. Biotechnol.* **2014**, *32*, 773.

34. J. J. Kim, L. Hou, N. F. Huang, *Acta Biomater.* **2016**, *41*, 17.

35. R. Walser, W. Metzger, A. Gorg, T. Pohlemann, M. D. Menger, M. W. Laschke, *Eur. Cell Mater.* **2013**, *26*, 222.

36. L. Pfisterer, T. Korff, *Methods Mol. Biol.* **2016**, *1430*, 167.

37. W. L. Haisler, D. M. Timm, J. A. Gage, H. Tseng, T. C. Killian, G. R. Souza, *Nat. Protoc.* **2013**, *8*, 1940.

38. Y. Zhang, G. L. Thomas, M. Swat, A. Shirinifard, J. A. Glazier, *PLoS. One.* **2011**, *6*, e24999.

39. R. J. McMurtrey, *Tissue Eng Part C. Methods.* **2016**, *22*, 221.

40. A. N. Mehesz, J. Brown, Z. Hajdu, W. Beaver, J. V. da Silva, R. P. Visconti, R. R. Markwald, V. Mironov, *Biofabrication.* **2011**, *3*, 025002.

41. T. Anada, J. Fukuda, Y. Sai, O. Suzuki, *Biomaterials.* **2012**, *33*, 8430.

42. J. C. Mombach, J. A. Glazier, R. C. Raphael, M. Zajac, *Phys. Rev. Lett.* **1995**, *75*, 2244.

43. R. A. Foty, M. S. Steinberg, *Wiley. Interdiscip. Rev. Dev. Biol.* **2013**, *2*, 631.

44. D. Shweiki, M. Neeman, A. Itin, E. Keshet, *Proc. Natl. Acad. Sci. U. S. A.* **1995**, *92*, 768.

45. C. F. Whittington, M. C. Yoder, S. L. Voytik-Harbin, *Macromol. Biosci.* **2013**, *13*, 1135.

46. A. V. Sterpetti, A. Cucina, L. S. D'Angelo, B. Cardillo, A. Cavallaro, *J. Cardiovasc. Surg. (Torino)*. **1992**, *33*, 619.

47. T. Xu, K. W. Binder, M. Z. Albanna, D. Dice, W. Zhao, J. J. Yoo, A. Atala, *Biofabrication.* **2013**, *5*, 015001.